Batch Grinding Kinetics and Particle Shape of Active Pharmaceutical Ingredients by Fluidized-bed Jet-milling

Tadashi Fukunaka [a,], Boris Golman [b], Kunio Shinohara [b]*

[a] Banyu Pharmaceutical CO., LTD. 9-1, Kamimutsuna 3-Chome, Okazaki, Aichi 444-0858, Japan

[b] Division of Chemical Process Engineering, Graduate School of Engineering, Hokkaido University, Nishi 8, Kita 13, Kita-ku, Sapporo, Hokkaido 060-8628, Japan

Abstract

As most of active pharmaceutical ingredients (APIs) developed in pharmaceutical industries have low solubility in water, production of fine particles by milling is performed for the main purpose of improvement of their dissolution rate. For low solubility APIs, or APIs for specialized formulations such as inhaled delivery, particle size requests are often in the 5-10 micron range.

Quite often, the selection of process parameters to achieve a desired milling endpoint is done empirically rather than through engineering approaches. Fluidized-bed jet-mills are relatively new to the pharmaceutical industry compared to loop-style jet-mills and pin-mills. Two of the merits of fluidized-bed jet-mills are less deterioration of API's quality due to thermal effect (e.g. melt-back) and less shut-down due to compaction over the internal surfaces during the long operation. Though it is known that the grinding mainly depends on inter-particle collision due to jet stream of gas, the grinding characteristics of API in this mill have not been investigated in detail.

The present objectives are to analyze the grinding mechanism and to find out the effect of the operating parameters on the breakage and selection functions and on the particle shape by the batch grinding test with a model API, Ethenzamide, in the fluidized-bed jet-mill.

Results of this study show that the variation of the residual fraction with the grinding time during milling can be expressed by a mathematical model using only the first Kapur function to be consistent with experimental data satisfactorily. The shape of the function was characteristic of API and well fitted to a cubic equation with respect to logarithmic particle diameter. The first Kapur function was found to be affected by such operating parameters as the grinding gas pressure, the charge weight of raw material and the linear velocity at the grinding nozzle. Although, under the low grinding pressure, the selection function tends to decrease with increasing charge weight, it was found to increase with decreasing charge under the high pressure. At the same gas flow rate, the selection function increases with the linear gas velocity.

According to the assessments of the breakage and the selection functions derived from the first Kapur function, it was found that the grinding of Ethenzamide was mainly caused

by attrition, where small fragments are scraped off from the surface of the large particle. This is considered to result from the physical property of Ethenzamide, as it is expected that organic compounds are difficult to yield volumetric fracture because they have higher elastic properties than inorganic compounds.

Shape index was also applied to the analysis of the mechanism. It describes a macroscopic shape of a particle outline using the ratio of minor- to major-axis of ellipse which is derived by Fourier transformation. The shape index of product particles by batch-grinding with the fluidized-bed jet-mill was found to increase with the grinding gas flow rate. Since higher gas flow rate leads to larger product particle size at a constant speed of the classifier rotor, the product particles are considered to become more spherical due to the selective grinding of large particles.

Keywords: Fluidized-bed jet-mill; Kinetics; Batch grinding; Mathematical model; Ethenzamide; Particle shape

* Corresponding author. Tel.: +81-564-57-1765; Fax: +81-564-57-1766.
E-mail address: tadashi_fukunaka@merck.com (T. Fukunaka).

1. Introduction

Since most of APIs developed in pharmaceutical industries have low solubility in water, production of fine particles by milling has been performed to increase the specific surface for the purpose of improving the solubility. Recently, the requirements for properties of milled particles, such as mean particle diameter and particle size distribution, are getting stricter and stricter.

However, the API milling process has not been developed so far on engineering approach, but on the past experiences mainly. In the pharmaceutical field, the fluidized-bed jet-mill is relatively new equipment comparing with the conventional equipments, such as a Jet-mill and a Pin-mill. One of the merits is less troubles like the deterioration of API's quality due to thermal effect (e.g. melt-back) and the shut-down due to compaction over the internal surfaces which is caused by the long operation, since the grinding mainly depends on inter-particle collision due to jet stream of gas (Fukunaka et al., 2003).

Concerning the fluidized-bed jet-milling, a few studies have been performed in recent years. Heng et al. (2000) and Chan et al. (2002) worked qualitatively on the effect of the operating parameters on the size distribution and the shape of lactose particles. Berthiaux and Dodds (1999) and Berthiaux et al. (1999) investigated batch and continuous grinding kinetics of alumina hydrate. However, the batch grinding kinetics of API, which is adhesive and agglomerative peculiar to pharmaceuticals, has not been investigated yet. Furthermore, the mathematical model of continuous operation which is important for optimization of pharmaceutical industrial grinding process should be based on the batch grinding one.

The objects of this paper are to analyze the grinding mechanism and to investigate the effect of the operating parameters of fluidized-bed jet-mill on the breakage and the selection functions by batch grinding test with a representative model API, Ethenzamide.

2. Theoretical considerations

Based on Kapur (1970) model on batch grinding, Berthiaux and Dodds (1999) developed a simplified equation on the variation of oversize fraction, $R(x,t)$, with grinding time, t, as:

$$R(x,t) = R(x,0)\exp\left[\sum_{k=1}^{p} K^{(k)}(x)\frac{t^k}{k!}\right] \quad (1)$$

Here the terms in the square bracket are called 'Kapur functions' including the complicated breakage and selection functions.

Thus, the ratio of oversize fraction at time, t, and initial one is defined as a residual ratio, $f(x,t)$, by equation (2). It characterizes the proportion of particles not to be subjected to the grinding action at t.

$$f(x,t) = \frac{R(x,t)}{R(x,0)} \quad (2)$$

The Kapur functions must be determined by fitting to the particle size distributions. In the case of short grinding time, however, equation (1) can be reduced to the following simplest equation by using only a first summation term for $k = 1$:

$$f(x,t) = \exp(K^{(1)}(x)t) \quad (3)$$

Furthermore, the breakage and selection functions can be derived from the first Kapur function (Berthiaux et al., 1996) as:

$$S_i = -K^{(1)}(x_i) \quad (4)$$

$$B_{ij} = \frac{S_{i-1} - S_i}{S_j} \quad (5)$$

where j denotes the size class of particles to be ground and i denotes the size class of particles to be produced by grinding j size class of particles.

As it is considered to give a practical quantitative way of description of pharmaceutical grinding process, these equations based on equation (1) are assumed to be applied to the case of fine particles which have adherent and agglomerative properties as API.

3. Materials and methods

3.1. Raw Material

Ethenzamide particles ($C_9H_{11}NO_2$: MW 165.19, 1.25 g/cm^3, IWAKI SEIYAKU CO., LTD.) were used as a raw material which are needle shaped and highly cohesive. The SEM photograph of particles and their size distribution are shown in Figs 1 and 2, respectively.

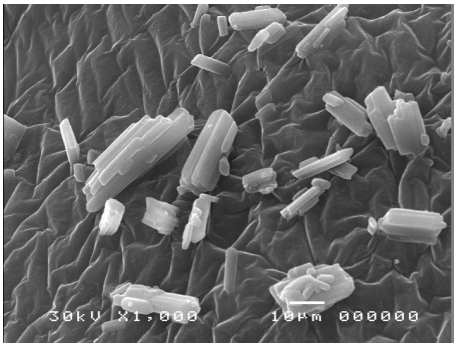

Fig. 1. SEM photograph of Ethenzamide particles

3.2. Grinding equipment

Fluidized-bed jet-mill (HOSOKAWA MICRON Corp. Counter Jet-mill 100 AFG) was used in the experiments, as schematically illustrated in Fig. 3. The grinding chamber consists of a cylindrical part with 97.4 mm inside diameter and a conical bottom, and the total volume is 950 cm^3. Three grinding nozzles of 1.9 or 3.0 mm in opening diameter are located horizontally at 120 degree intervals in the bottom of ca. 162 mm from the center of the classifier rotor. The raw material was fed into the chamber from the top by a screw feeder, and is accelerated by nitrogen gas compressed up to 0.60 MPa from the three nozzles to meet at the same point. The milled particles are classified by 50 ATP turbo-selector (50 mm outside diameter,

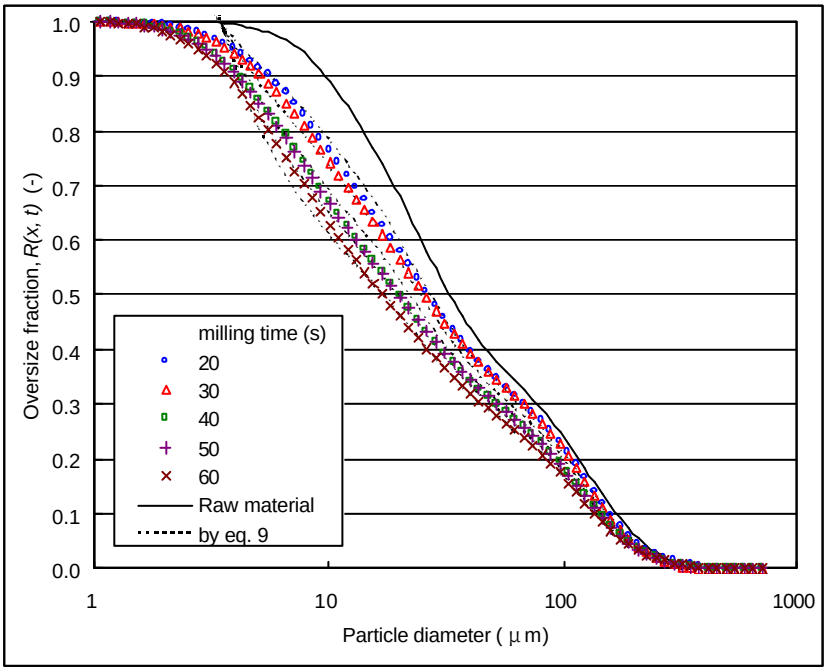

Fig. 2. Particle size distributions of raw material and inside samples for Run#1

maximum rotor speed: 22000 rpm) which is located above the chamber. The classified fine particles leaving the grinding chamber are collected as a product in a bag-filter. The rejected coarse particles at the classifier are re-circulated in the chamber until they are ground into smaller size than a certain size to pass through the classifier rotor. The nitrogen passed through the filter is vented to atmosphere with a blower via HEPA filter.

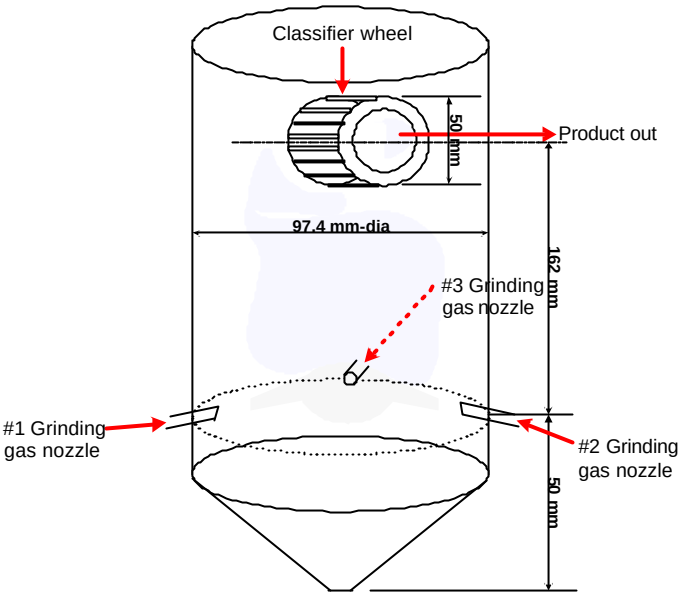

Fig. 3. Schematic illustration of fluidized-bed jet-mill

3.3. Batch grinding experiment

Fig. 4 shows the schematic diagram of experimental setup. To perform batch grinding experiment, the material feed is cut off by installing a plug plate on the top of the chamber. A given weight of particles is put in the mill initially and the classifier is set to a maximum speed of rotation of 22000 rpm to keep the particles inside the mill as much as possible. Although small amount of fine particles left the chamber during the experiment, it was unavoidable due to the scheme of equipment. Experiments were performed under the blower control by keeping the pressure inside the mill –0.3 kPa in any conditions. The grinding time was 60 sec and the system was shut down at 10 sec intervals to take a portion of the milled sample collected at the bottom of the mill. Sampling was started after 20 sec to avoid scattering of data of particle size distribution. The experiments were performed within practical

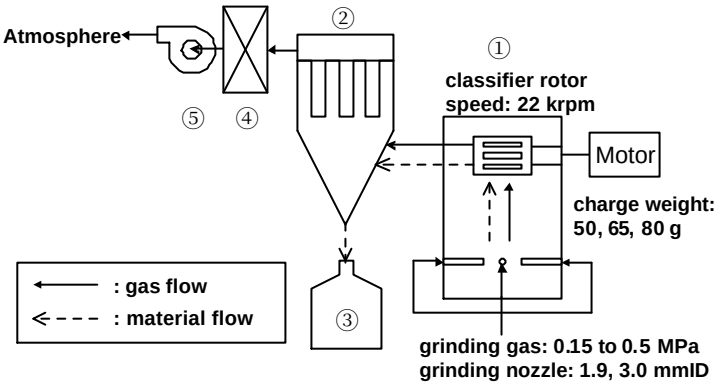

①Fluidized-bed jet-mill, ②Bag filter, ③Product-recovery pot, ④HEPA filter, ⑤Blower

Fig. 4. Experimental setup for fluidized-bed jet-mill

Table 1. Experimental conditions and results by batch grinding

Run#	nozzle dia. d_N (mm)	gas press. P (MPa)	gas flow rate Q (m3/min)	charge weight W (g)	averaged shape index: K_{av} (—)	mean particle dia.: X_m (μm)
Raw material	-	-	-	-	0.497	29.8
1	1.9	0.3	0.40	80	0.641	4.6
2	1.9	0.4	0.51	80	0.636	5.1
3	1.9	0.3	0.40	65	-	-
4	1.9	0.3	0.40	50	0.639	4.5
5	1.9	0.5	0.59	80	0.647	4.8
6	3.0	0.18	0.70	80	0.668	5.8
7	3.0	0.18	0.70	50	0.682	5.5
8	3.0	0.15	0.63	50	0.643	6.0
9	3.0	0.15	0.63	80	0.659	5.4
10	1.9	0.5	0.59	50	0.671	4.1
11	1.9	0.4	0.51	65	-	-
12	1.9	0.4	0.51	50	0.619	4.1
13	1.9	0.5	0.59	65	-	-

range of operating parameters such as the charge weight, the grinding gas pressure and the grinding nozzle diameter, as shown in Table 1.

3.4. Particle size distribution

The particle size distribution was measured by means of a wet-type laser diffraction analyzer (MICROTRACK HRA Model#6320-X100, NIKKISO Co., Ltd). The sample was set up by suspending particles in the 10 mL of Isopar-G (ExxonMobil Chemical) with 0.25 wt% lecithin (Wako Pure Chemical Industries, Ltd.) as a dispersant and measured under deaggregation condition after sonication.

3.5. Particle shape analysis

Particle shape analysis (Otani, M. et. al., 1995) was performed by Fourier transformation of each point on the circumference of the projected particle image on rectangular coordinates, after a SEM photograph of the particle sample was first digitized and then binarized to extract the particle outline using image analysis software, Optimas (Media Cybernetics, version 6.5). The shape index of each particle was defined as the ratio of minor- to major-axis of the approximate ellipse which is obtained by using Fourier coefficients. The representative shape index, K_{av}, of the sample in this paper is the arithmetic mean value of indices measured for approximately 100 particles.

4. Results and discussion

4.1. Variation of residual ratio with time

The oversize fraction of particles during milling, $R(x,t)$, is expressed by total mass balance with particle size distributions of samples collected inside and outside the mill as follows:

$$R(x,t) = \frac{(W_{ini} - W_{clf} - W_{clc})}{W_{ini}} R_{mill}(x,t) + \frac{W_{clf}}{W_{ini}} R_{clf}(x) + \frac{W_{clc}}{W_{ini}} R_{clc}(x) \qquad (6)$$

where W is the weight of sample, subscripts "ini", "$mill$", "clf" and "clc" mean initial charge, sample in the mill, samples collected from the filter and in the recovery pot of the bag-filter, respectively. In the present experiment, a part of coarse particles (subscript "clc") to be retained inside, was discharged outside the mill with the product fine particles

(subscript " clf ") which were classified appropriately. The total amounts of samples collected in the bag, $W_{clf}+W_{clc}$, was around 20 to 40 % of that of the charge weight. Consequently, it is taken into account on the particle size distribution by equation (6). On the other hand, although the amount of the overflow is reduced by smaller charge weight, ranges of present experiment are considered as appropriate, because the grinding kinetics can not be evaluated in the case of the dilute particle concentration inside the mill.

Fig. 2 shows the variation of the oversize fraction with time for Run#1. It is found that the distribution shifts to the left with time. Assuming that the grinding time is short, the variation of residual ratio with time for arbitrary particle size x_i in the distribution is simplified using equation (3):

$$f(x_i,t)=\exp(K^{(1)}(x_i)t) \qquad (7)$$

Therefore, the first Kapur function is obtained as the slope of the straight line by plotting t vs $\ln\{f(x_i,t)\}$. As a typical result, Fig. 5 shows the variation of the residual ratio with time for Run#1. In any fraction, the residual ratios linearly decrease with time to fit to equation (7). Since these trends were observed in all runs and the correlation coefficients, R^2 values, were more than 0.8, it was concluded that the influence of discharge of particles on the grinding process was comparatively small and the grinding time of present experiment was within the range to be applied to equation (7). Hereafter, the first Kapur function is thus obtained from the slope.

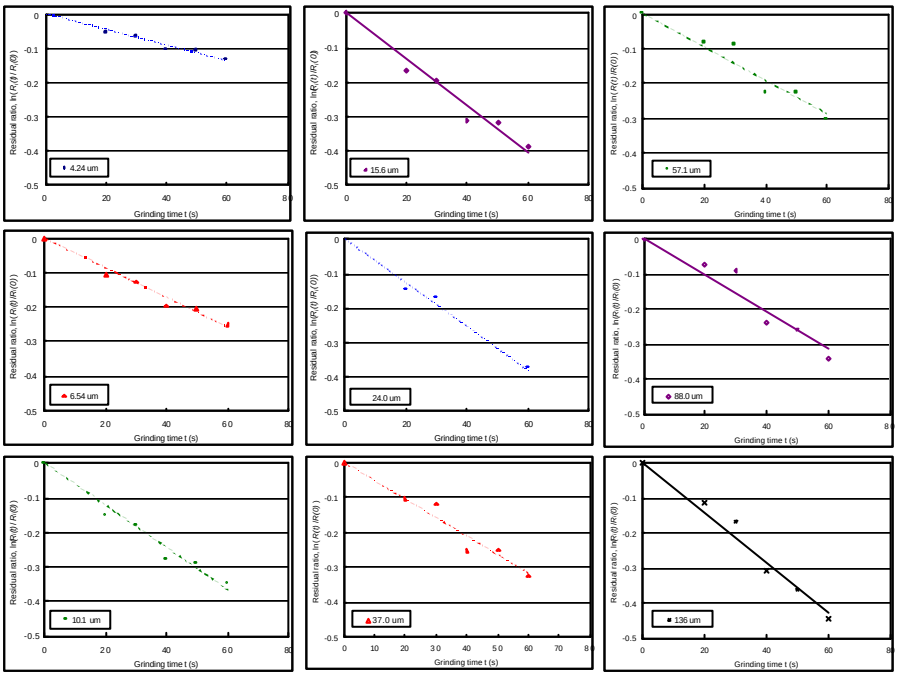

Fig. 5. Data fitting of residual ratio to grinding time by batch grinding

4.2. Variation of first Kapur function with particle size

Figs. 6 to 9 show the variations of the first Kapur function obtained in the previous

section with particle size. As the y-axis shows the negative value of selection function as expressed by equation (4), it means that the larger absolute value leads to higher probability to be ground. In this section, the first Kapur function is discussed as a selection function. The trends that the selection function was reversed in the range of 20 to 50 µm due to two inflection points were observed. The grinding mechanism is considered to be peculiar to API, because these are much different from the results using alumina hydrate (Berthiaux and Dodds, 1999). The details are discussed later.

Figs. 6 to 8 show the effect of the charge weight on the selection function for grinding with 1.9 mm-diameter nozzle under different grinding gas pressure of 0.3, 0.4 and 0.5 MPa, respectively. At the lower pressure (0.3 MPa), the selection function tends to increase with a decrease in the charge weight, because the grinding process is considered to be controlled by the grinding energy per unit weight rather than the collision probability. On the other hand, the selection function reaches a minimum at 65 g of the charge weight at higher pressure (0.4 and 0.5 MPa), because it is considered that as the increase in the collision probability with the charge weight is more significant than the decrease in the grinding energy per unit weight.

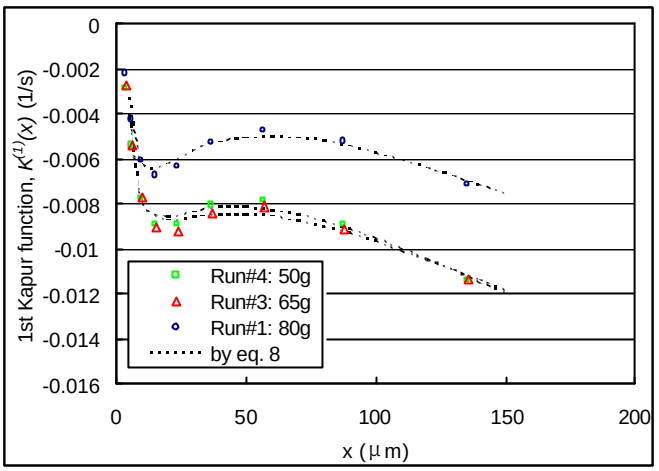

Fig. 6. Effect of charge weight on 1st Kapur function at 0.3 MPa with 1.9 mm-diameter nozzle

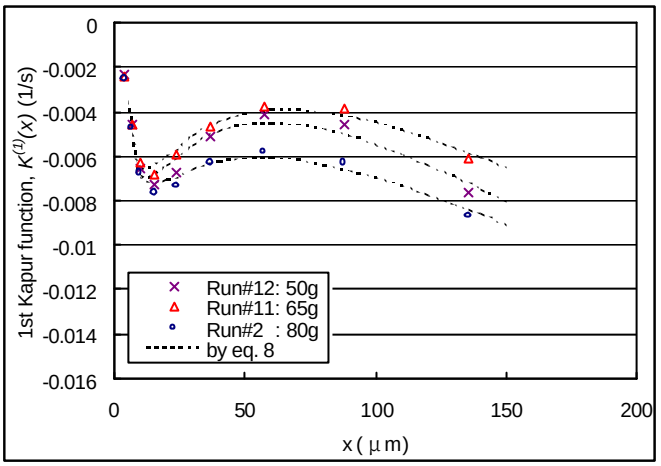

Fig. 7. Effect of charge weight on 1st Kapur function at 0.4 MPa with 1.9 mm-diameter nozzle

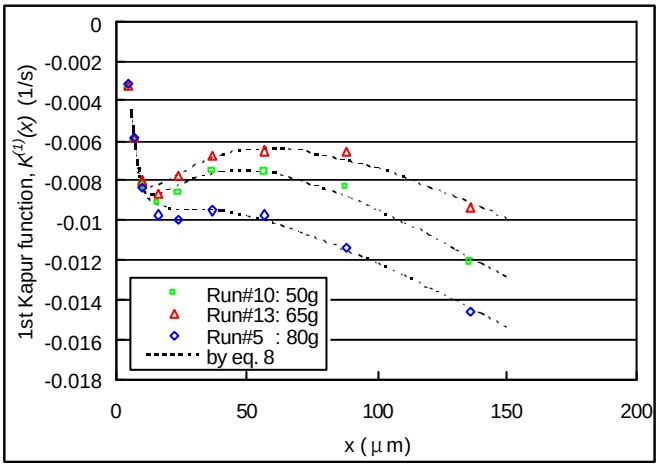

Fig. 8. Effect of charge weight on 1st Kapur function at 0.5 MPa with 1.9 mm-diameter nozzle

Fig. 9 also illustrates the effects of the charge weight and the grinding pressure using 3.0 mm-nozzle on the selection function. As shown in Table 1, the grinding gas flow rate at 0.15 MPa is almost the same as that at 0.5 MPa using 1.9 mm-nozzle. In the graph, it is found that higher pressure and smaller charge lead to higher value of selection function due to the same reason as shown in Fig. 6. Furthermore, comparing Run# 5, 8 and Run#9, 10

at the same gas flow rate, respectively, it is considered that the linear gas velocity much contributes to the increase in the selection function as compared with the gas flow rate.

The attempt to express the first Kapur function as a numerical formula was performed. Tanaka (1972) assumed that the selection function for jet-mill was in proportion to an exponent of particle size. In this paper, similarly to their power law dependence of selection function on particle size, a cubic equation by equation (8) is proposed considering both the graph shape and the physical meanings.

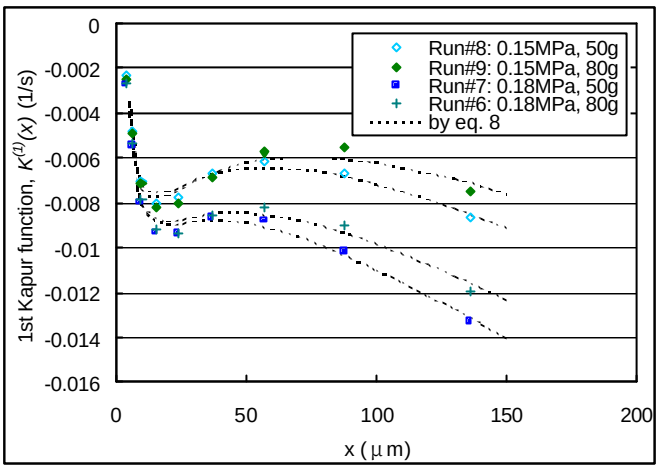

Fig. 9. Effects of charge weight and grinding pressure on 1st Kapur function with 3.0 mm-diameter nozzle

$$K^{(1)}(x) = a(\ln(x))^3 + b(\ln(x))^2 + c(\ln(x)) + d \qquad (8)$$

It is considered that the selection function is affected by 3 primary factors as 1) collision energy which particles hold, 2) probability of existence of particles which can collide with and 3) particle size. These correspond to the cubic, quadratic and simple terms of equation (8), respectively. Tanaka (1972) considered that the rate constant was proportional to the probability of collisions of the particles injected into the jet and the kinetic energy of unit mass of particles hitting each other. Therefore, the cubic and the quadratic terms in equation (8) are considered to correspond to the collision energy and the collision probability of particles, respectively. The probability seems to be proportional to the projected area of particles drawn into the jet stream from the nozzles. For the simple term, according to Rittinger's law (1967), the surface energy (= specific surface area) which particles hold increases with progress of grinding, and is in inverse proportion to the particle size. That is to say, it is considered that the particle size

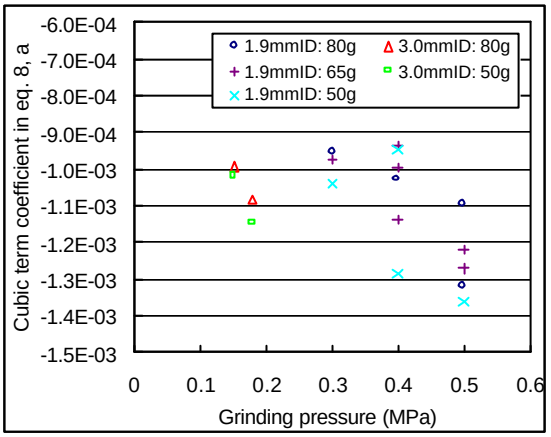

Fig. 10. Variation of cubic term coefficient in equation (8) with grinding pressure

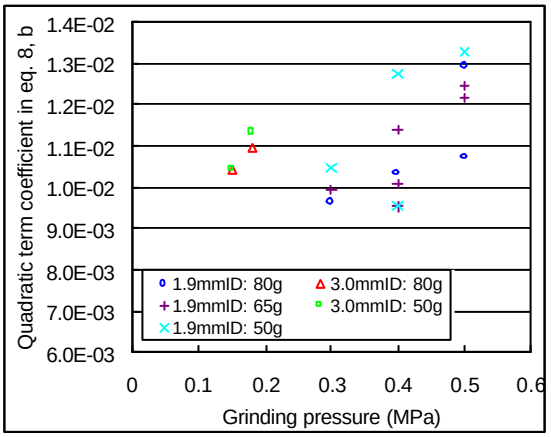

Fig. 11. Variation of quadratic term coefficient in equation (8) with grinding pressure

corresponds to the surface energy, and the larger particle is, the easier it is ground.

Figs. 6 to 8 show the results of calculation by equation (8). Since the calculated lines are fitted to the experimental results well, the assumption described above is considered to be appropriate. For all the runs, the coefficients and the constant in equation (8) obtained by fitting to experimental data are shown in Table 2 and R^2 values are more than 0.9.

4.3. Influence of operating parameters on selection function

Figs. 10 to 13 represent the influence of the operating parameters on the selection function. The coefficients and the constant shown in Table 2 are plotted for the pressure, and the parameters are the charge weight and the nozzle diameter. In the graphs, a certain correlations among them are observed. For the third coefficient, a, which relates to the collision energy in Fig. 10, the absolute value increases with an increase in the pressure and a decrease in the charge. Consequently, it contributes to an increase in the selection function. This result meets with the general influences of the pressure and the charge on the grinding performance of conventional jet-mills. For the second coefficient, b, which relates to the collision probability in Fig. 11, the value also increases with the pressure and a decrease in the charge. However, as it contributes to a decrease in the selection function due to the positive sign, these results explain why the particle bed-density decreases with an increase in the pressure and increases with the charge, respectively. For the first coefficient, c, which relates to the surface energy in Fig. 12, it is found to be the same tendency as that of the coefficient, a. This also meets with the results that the energy increases with the progress of the grinding process according to an increase in the pressure and a decrease in the charge. For the constant, d, in Fig. 13, it is found to be the same tendency as that of the coefficient, b.

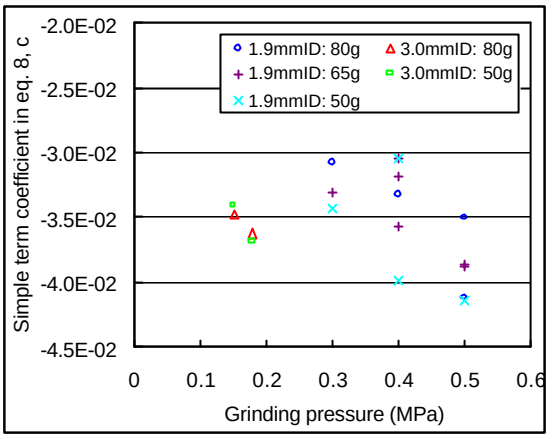

Fig. 12. Variation of simple term coefficient in equation (8) with grinding pressure

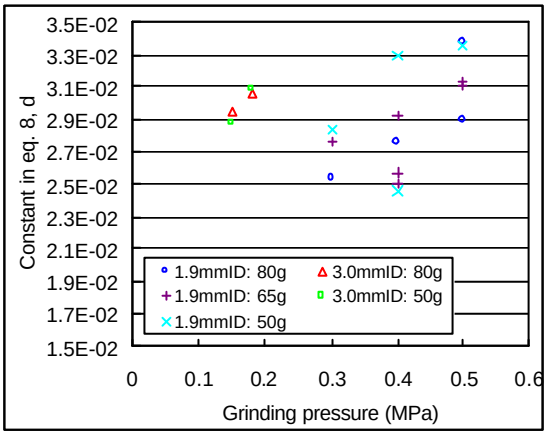

Fig. 13. Variation of constant in equation (8) with grinding pressure

Table 2. Results of curve-fitting for 1st Kapur function

Run#	R^2 value	Coefficients and constant in equation (8)			
		a	*b*	*c*	*d*
1	0.956	-9.555E-04	9.624E-03	-3.080E-02	2.535E-02
2	0.953	-1.027E-03	1.033E-02	-3.331E-02	2.750E-02
3	0.976	-9.754E-04	9.923E-03	-3.312E-02	2.765E-02
4	0.976	-1.044E-03	1.047E-02	-3.433E-02	2.832E-02
5	0.987	-1.094E-03	1.073E-02	-3.512E-02	2.887E-02
6	0.970	-1.086E-03	1.097E-02	-3.628E-02	3.056E-02
7	0.981	-1.147E-03	1.133E-02	-3.693E-02	3.083E-02
8	0.964	-1.021E-03	1.043E-02	-3.420E-02	2.875E-02
9	0.935	-9.949E-04	1.044E-02	-3.474E-02	2.938E-02
10	0.971	-1.362E-03	1.327E-02	-4.154E-02	3.348E-02
11	0.939	-1.137E-03	1.140E-02	-3.571E-02	2.917E-02
12	0.910	-1.287E-03	1.277E-02	-3.984E-02	3.291E-02
13	0.964	-1.220E-03	1.218E-02	-3.857E-02	3.107E-02

4.4. Bacth grinding model for API

Substitution of equation (8) into equation (7) gives equation (9), which expresses the residual ratio with particle size, x, at time, t, after batch grinding. As a typical result, Fig. 14 depicts the experimental results of the residual ratio of Run#1 and calculated lines obtained by equation (9). Since the calculated lines fitted to the experimental data well, the mathematical model for the batch grinding of API is found to be appropriate. Fig. 2 shows the calculated results of the variation of residual ratio with time obtained by equation (9). Although the calculated lines are almost fitted to the experimental data at each grinding time for wide range of particle sizes, equation (8) could not be used for fitting raw data for particles smaller then 4 μm due to the divergence of calculated values. This issue is caused by the functional form of this equation defining the first Kapur function as a logarithmic function of particle size. Considering the unique shape of the first Kapur function, as shown in Figs. 6 to 9, equation (9) is applicable to the simple simulation of the variation of residual ratio with grinding time during batch grinding of API.

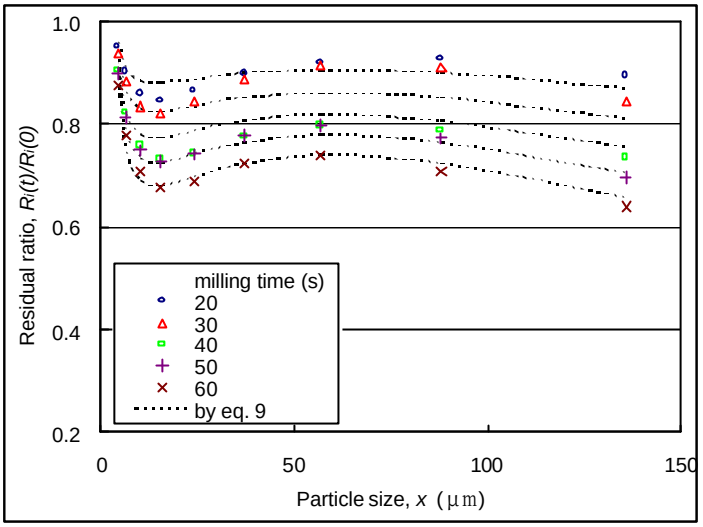

Fig. 14. Fitting of batch grinding data by equation (9)

$$f(x,t) = \exp[\{a(\ln(x))^3 + b(\ln(x))^2 + c(\ln(x)) + d\}t] \qquad (9)$$

4.5. Assessment of Breakage Mechanism

4.5.1. Breakage and selection functions

Approximating the grinding data by the first Kapur function, the breakage and the selection functions can be expressed by equations (4) and (5), respectively. As a typical result, the following breakage B and selection S matrices of Run#1 are obtained by dividing the particle size range into 10 classes in the geometric

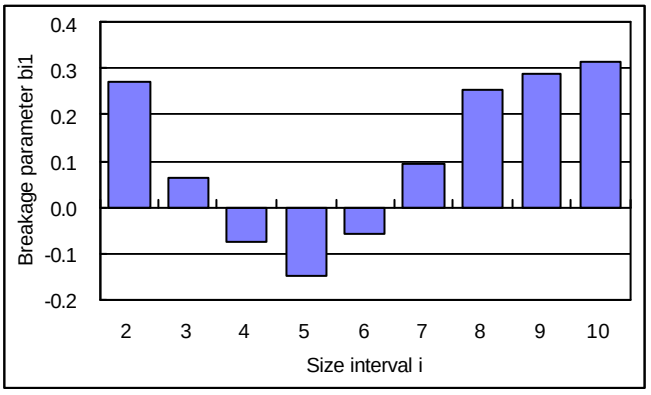

Fig. 15. Mass distribution of fragments produced by breakage of particles of class 1 size

progression, as summarized in Tables 3 and 4.

Table 3. Classification of particle size range

Particle class (i, j)	Particle size range (μm)
1	>136
2	88.0 - 136
3	57.1 - 88.0
4	37.0 - 57.1
5	24.0 - 37.0
6	15.6 - 24.0
7	10.1 - 15.6
8	6.54 - 10.1
9	4.24 - 6.54
10	<4.24

Table 4. Matrices of *S* and *B* calculated

$$S = \frac{1}{100}\begin{bmatrix} 0.7162 & 0.5248 & 0.4790 & 0.5314 & 0.6371 & 0.6779 & 0.6106 & 0.4315 & 0.2267 & 0.0000 \end{bmatrix}$$

$$B = \begin{bmatrix} & j=1 & 2 & 3 & 4 & 5 & 6 & 7 & 8 & 9 & 10 \\ i=1 & 0 & 0 & 0 & 0 & 0 & 0 & 0 & 0 & 0 & 0 \\ 2 & 0.267 & 0 & 0 & 0 & 0 & 0 & 0 & 0 & 0 & 0 \\ 3 & 0.064 & 0.087 & 0 & 0 & 0 & 0 & 0 & 0 & 0 & 0 \\ 4 & -0.073 & -0.100 & -0.109 & 0 & 0 & 0 & 0 & 0 & 0 & 0 \\ 5 & -0.148 & -0.201 & -0.221 & -0.199 & 0 & 0 & 0 & 0 & 0 & 0 \\ 6 & -0.057 & -0.078 & -0.085 & -0.077 & -0.064 & 0 & 0 & 0 & 0 & 0 \\ 7 & 0.094 & 0.128 & 0.141 & 0.127 & 0.106 & 0.099 & 0 & 0 & 0 & 0 \\ 8 & .250 & 0.341 & 0.374 & 0.337 & 0.281 & 0.264 & 0.293 & 0 & 0 & 0 \\ 9 & 0.286 & 0.390 & 0.428 & 0.385 & 0.321 & 0.302 & 0.335 & 0.475 & 0 & 0 \\ 10 & 0.317 & 0.432 & 0.473 & 0.427 & 0.356 & 0.334 & 0.371 & 0.525 & 1.000 & 1.000 \end{bmatrix}$$

When S is set as above, B_{ij} is calculated by equation (5) as follows: For example, at first, when j is given as one, B_{21} is given as $\frac{S_1 - S_2}{S_1}$. According to the same procedure, B_{31} to B_{101} are calculated. Next, when j is given as two, B_{32} is given as $\frac{S_2 - S_3}{S_2}$. Then, the same iterations are performed up to B_{109}.

For the selection matrix, the selection function tends to increase with the particle size, because it is considered that larger particles are easier to be ground corresponding to the first Kapur function. Only for the fractions from i = 3 to 6, however, the trends are reversed. Fig. 15 shows the mass distribution by focusing on the largest particle class (j = 1) in the breakage matrix. In the graph, the fractions from i = 4 to 6 are observed to be of negative values. As it is unavoidable for them to be negative in the form of equation (5), they are assumed to be non-breakable fractions. It is found that the small particles up to 10.1 μm (i = 7 to 10) and the large particles from 88 to 136 μm (i = 2) are milled selectively. As this trend is common to all runs, it is presumed that the grinding mechanism of Ethenzamide by fluidized-bed jet-milling mainly does not depend on the massive fracture that a large particle is divided into a few pieces, but on the attrition that small fragments are scraped off from the surface of a large particle, due to the physical property of organic compounds which have higher elastic properties than inorganic ones (Ragnarson and Sjogren, 1985).

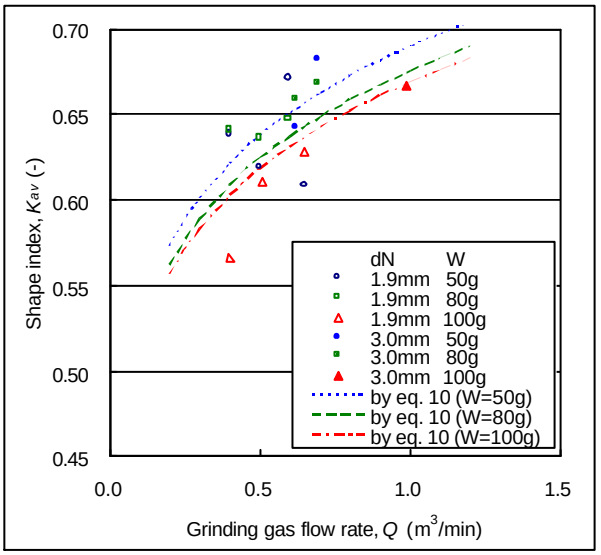

Fig. 16. Effect of grinding gas flow rate on K_{av}

4.5.2. Particle shape index

The values of shape indices and the mean particle diameters of milled particles are shown in Table 1. Figs. 16 and 17 show the effect of the grinding gas flow rate on the shape index and the mean particle diameter, respectively. The gas flow rate was used in these figures to combine the effects of the nozzle diameter and the gas pressure. It is found that both the index and the mean diameter increase with in an increase in the gas flow rate. It is considered that as the grinding proceeds due to an increase in the grinding energy which is caused by an increase in the gas flow rate, spheroidizing the particles results in an increase in the shape index.

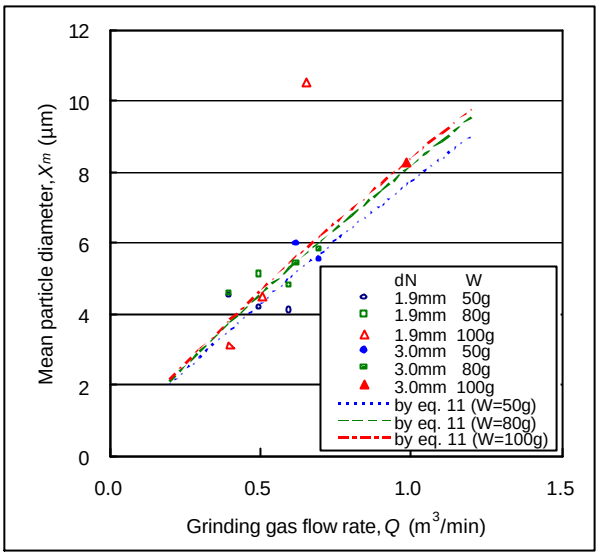

Fig. 17. Effect of grinding gas flow rate on X_m

For the mean particle diameter, in narrow range of the flow rate, it increases with a decrease in grinding energy. When the gas flow rate increases drastically, however, the mean diameter also increases to follow the increase in the critical diameter of particles classified by a mechanical rotor classifier.

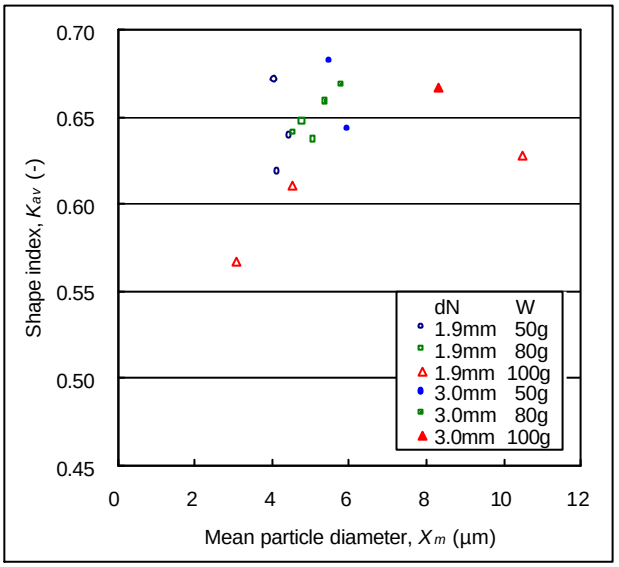

Fig. 18. Relationship between X_m and K_{av}

Furthermore, the shape index and the mean particle diameter are expressed as the following experimental equations with the gas flow rate and the charge weight as variables, respectively, and each coefficient was obtained by least-square method.

$$K_{av} = a_1 \times Q^{b_1} \times (W/100)^{c_1} \quad (10)$$

$$a_1 = 0.6688,\ b_1 = 0.1139,\ c_1 = -0.04448$$

$$X_m = a_2 \times Q^{b_2} \times (W/100)^{c_2} \quad (11)$$

$$a_2 = 8.362,\quad b_2 = 0.8484,\quad c_1 = 0.1138$$

The dotted and dashed lines in Figs. 16 and 17 are the calculated results. Comparing

the coefficients, it is found that the gas flow rate influences both K_{av} and X_m largely.

Fig. 18 shows the relationship between X_m and K_{av}. They are found to be in proportional relationship within the present experimental range, since the product particles are considered to become more spherical due to the selective grinding of large particles. Consequently, this result supports the batch grinding mechanism according to the assessments of the breakage and selection functions in previous section.

5. Conclusions

The batch grinding kinetics and mechanism of Ethenzamide as a representative API by fluidized-bed jet-milling were investigated. As the result, the following findings were made:

1) The variation of the residual ratio with the grinding time for each particle class during milling was expressed by equation (7) using only the first Kapur function. The graph shape of the function with particle size was much different from inorganic compounds, characteristic to API and fitted well to the cubic function expressed by equation (8).

2) The selection function derived from the first Kapur function was found to be affected by the operating parameters as the grinding gas pressure, the charge weight and the linear gas velocity at the grinding nozzle. Although, under low grinding pressure, the selection function tends to decrease with the increase in the charge weight, it was found to increase with the decrease in the charge under high pressure. At the same gas flow rate, the selection function increases with the linear gas velocity.

3) The mathematical model expressed by equation (9) for the batch grinding was consistent with experimental data satisfactorily.

4) According to the assessments of the breakage and selection functions, the grinding mechanism of Ethenzamide was supposed to depend mainly on particle attrition that small fragments are scraped off from the surface of a big particle due to the physical property of organic compounds which have higher elastic properties than inorganic ones.

5) Both the shape index and the mean particle diameter of product increase with an increase in the gas flow rate. They are in proportional relationship within the present experimental range. As the results, the product particles are considered to become more spherical due to the selective grinding of large particles. This result supports the batch grinding mechanism by analyzing the breakage and selection functions.

Nomenclature

a , b , c , d	:	Coefficients and constant in equation (8)	
a_1 , b_1 , c_1	:	Coefficients in equation (10)	
a_2 , b_2 , c_2	:	Coefficients in equation (11)	
B	:	Breakage function as matrix	
d_N	:	Grinding nozzle diameter	(mm)
$f(x,t)$	:	Residual ratio related to particle size x at time t	
$K^{(1)}(x_i)$	:	1st order Kapur function	(1/s)
K_{av}	:	Averaged shape index	
k	:	integer constant in equation (1)	
P	:	Grinding gas pressure	(MPa)
Q	:	Grinding gas flow rate	(m^3/min)
$R(x,t)$	:	Oversize fraction with respect to particle size x at time t	
$R\ (x)$	:	Oversize fraction with respect to particle size x	
S	:	Selection function as matrix	(1/s)
t	:	Grinding time	(s)
x , x_i	:	Particle sizes	(μm)
X_m	:	Mean particle diameter	(m)
W	:	Weight of particles	(g)

<Subscripts>

clc	:	Coarse particles leaving the mill
clf	:	Fine particles leaving the mill
i , j	:	Indices relative to size intervals
ini	:	Initial charge of raw material
$mill$	:	Particles remaining in the mill

References

Berthiaux, H. and Dodds, J., 1999. Modeling fine grinding in a fluidized bed opposed jet mill Part I: Batch grinding kinetics. Powder Technol., 106, 78-87.

Berthiaux, H., Chiron, C. and Dodds, J., 1999. Modeling fine grinding in a fluidized bed opposed jet mill Part II: Continuous grinding. Powder Technol., 106, 88-97.

Berthiaux, H., Varinot, C. and Dodds, J., 1996. Approximate calculation of breakage parameters from batch grinding tests. Chem. Eng. Sci., 51, 4509-4516.

Chan, L.W., Lee, C.C. and Heng, P.W.S., 2002. Ultrafine grinding using a fluidized bed opposed jet mill: Effects of feed load and rotational speed of classifier wheel on particle shape. Drug Dev. Ind. Pharm., 28, 939-947.

Fukunaka T and Tom, J. W., 2003. R&D of milling technology in pharmaceutical industry. J. Soc. Powder Technol. Japan, 40, 655-663.

Heng, P.W.S., Chan, L.W. and Lee, C.C., 2000. Ultrafine grinding using a fluidized bed opposed jet mill: Effects of process parameters on the size distribution of milled particles. J. Pharm. Sci., 10, 445-451.

Kapur, P.C., 1970. Kinetics of batch grinding: Part B. An approximate solution to the grinding equation. Trans. Soc. Min. Eng. AIME, 247, 309-313.

Otani, M., Minoshima, H., Uchiyama, T., Shinohara, K., Takayashiki, K. and Ura, T., 1995. The effect of particle shape on the mechanical properties of powder bed. J. Soc. Powder Tecnol., Japan, 32, 151-157.

Tanaka, T., 1972. Scale-up theory of jet mills on basis of comminution kinetics. Ind. Eng. Chem. Process Des. Develop., 11, 238-241.

Rittinger, Von PR. 1867. Lehrbuch der aufbereitungskunde in ihrer neusten entwicklung und ausbilding systematisch dargestellt. Ernst and Korn., Berlin.

Ragnarsson, G and Sjogren, J., 1985. Force-displacement measurements in tableting. J. Pharm. Pharmacol., 37, 145-150.